Coupling of phonons and electromagnons in GdMnO3

Andrei Pimenov, T. Rudolf, Franz Mayr, Alois Loidl, A. A. Mukhin, A. M. Balbashov

Coupling of phonons and electromagnons in GdMnO$_3$

A. Pimenov,[1] T. Rudolf,[1] F. Mayr,[1] A. Loidl,[1] A. A. Mukhin,[2,1] and A. M. Balbashov[3]

[1]*Experimentalphysik V, EKM, University of Augsburg, 86135 Augsburg, Germany*
[2]*A. M. Prokhorov General Physics Institute of the Russian Academy of Sciences, 119991 Moscow, Russia*
[3]*Moscow Power Engineering Institute, 105835 Moscow, Russia*

The infrared and terahertz properties of GdMnO$_3$ have been investigated as functions of temperature and magnetic field, with special emphasis on the phase boundary between the incommensurate and the canted antiferromagnetic structures. The heterogeneous incommensurate phase reveals strong magnetodielectric effects, characterized by significant magnetoelectric contributions to the static dielectric permittivity and by the existence of electrically excited magnons (electromagnons). In the commensurate canted antiferromagnetic phase the magnetoelectric contributions to the dielectric constant and electromagnons are suppressed. The corresponding spectral weight is transferred to the lowest lattice vibration, demonstrating the strong coupling of phonons with electromagnons.

PACS number(s): 75.80.+q, 63.20.Ls, 75.30.Ds, 75.47.Lx

Multiferroic materials with the simultaneous occurrence of magnetism and ferroelectricity are a hot topic in recent solid-state research. They provide interesting and spectacular physical properties and promise attractive applications.[1–3] Multiferroic behavior occurs in a variety of systems originating from very different physical mechanisms, including materials with independent magnetic and ferroelectric subsystems, like some boracites, Aurivillius phases, hexagonal manganites, and the lone-pair ferroelectrics with magnetic ions.[3] Recently sulfospinels with relaxorlike short-range ferroelectric (FE) order have been detected[4] with a strong coupling of the electric and magnetic properties at low frequencies. Finally, in the perovskite manganites there is robust experimental evidence[5,6] that the onset of helical magnetic order induces spontaneous FE polarization.[7,8] Dzyaloshinskii-Moriya-type interactions have been utilized to explain the ferroelectricity that is induced by the helical spin structure.[9–11] A similar spin-driven ferroelectricity is believed to be operative in Ni$_3$V$_2$O$_8$.[12]

After having established the ground-state properties of this interesting class of materials, a study of their dynamic properties will significantly enhance our knowledge of magnetoelectric (ME) coupling.[13] Magnons are the characteristic excitations of magnetic structures, while soft phonons as inferred by the Lyddane-Sachs-Teller relation condense at canonical ferroelectric phase transitions. It seems clear that soft phonons cannot be relevant excitations in the ferroelectric manganites, as (improper) ferroelectricity is induced by the magnetic order coupled to the lattice. Recently it has been shown that electromagnons are relevant collective modes in these materials.[14] Electromagnons are spin waves that are excited by an ac electric field. In TbMnO$_3$ and GdMnO$_3$ it has been documented that these new excitations exist not only in the magnetic phase characterized by the helical spin structure, but also in the longitudinally modulated (sinusoidal) structure, provided that a "helical-type" vector component of the spin wave is dynamically induced via the ac electric field.[14]

In this paper we present detailed investigations of the terahertz and far-infrared properties of GdMnO$_3$. We investigate electromagnons and phonons as functions of tempera-

ture and magnetic field. We provide striking experimental evidence that (i) electromagnons are strongly coupled to phonons with a considerable shift of optical weight between these excitations and (ii) electromagnons contribute considerably to the static dielectric constant.

Single crystals of GdMnO$_3$ have been prepared using the floating-zone method with radiation heating. The samples have been characterized using x-ray, magnetic, and dielectric measurements.[15] The basic properties of our samples agree well with the results obtained by other groups.[6,16] The experiments at terahertz frequencies were carried out in a Mach-Zehnder interferometer.[17] The absolute values of the complex dielectric permittivity $\varepsilon^* = \varepsilon_1 + i\varepsilon_2$ were determined directly from the measured spectra using the Fresnel optical formulas for the complex transmission coefficient. The spectra in the infrared frequency range have been obtained using a Bruker IFS-113 Fourier-transform spectrometer. The experiments in external magnetic fields were performed in a superconducting split-coil magnet with polypropylene windows allowing reflectance experiments to be carried out in magnetic fields up to 7 T.

The upper panel of Fig. 1 shows the *H-T* phase diagram of GdMnO$_3$ for $H \parallel c$ in the zero-field-cooled (ZFC) regime[14] which basically coincides with the diagrams published previously.[6,15] GdMnO$_3$ is paramagnetic above $T_N \simeq 42$ K and transforms into an incommensurate antiferromagnetic (IC-AFM) state below this temperature. Depending upon the value of the external magnetic field along the *c* axis, the magnetic state becomes canted antiferromagnetic (CA-AFM) below ~20 K. For $T < 9$ K and in low fields the spin structure reveals increasing complexity due to an additional ordering of the Gd subsystem. This region, which is indicated by a hatched area in the phase diagram of the upper panel of Fig. 1, is not further discussed in the course of this work. There is one important difference compared to the (H, T) phase diagram published in Ref. 15: under zero-field-cooling conditions no phase transition occurs and the CA-AFM state remains stable down to 9 K. This fact allows a switch between the magnetoelectric IC-AFM and the CA-AFM phases with very low fields. The incommensurate phase is especially
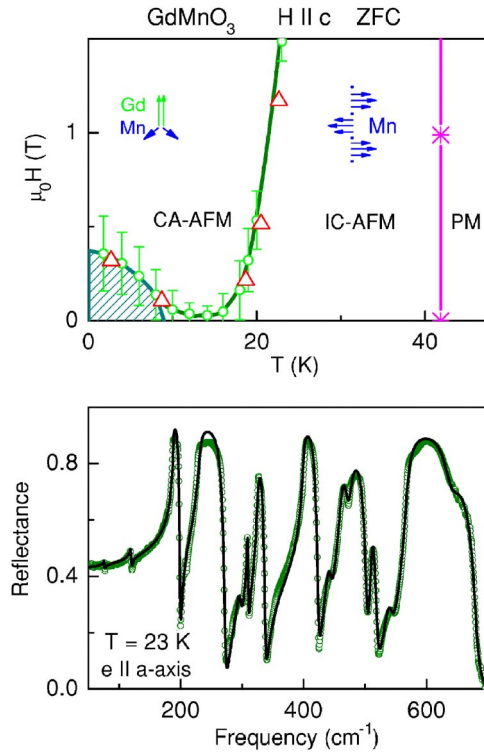
FIG. 1. (Color online) Upper panel: Magnetic phase diagram of GdMnO$_3$ for $H\|c$ for zero-field cooling. Circles and stars, results of magnetization measurements; triangles, data from dielectric experiments (Ref. 14). Lines are drawn to guide the eye. PM, paramagnetic; IC-AFM, incommensurate antiferromagnetic [probably sinusoidally modulated (Ref. 6)]; CA-AFM, canted antiferromagnetic structure. The hatched region indicates the ordering of the Gd sublattice. Lower panel: Reflectance of GdMnO$_3$ with polarization along the *a* axis and at phonon frequencies. Symbols, experiment; solid line, model calculation assuming a sum of 15 Lorentzians (see text).

interesting from the spectroscopic point of view, because unusual excitations of mixed magnetoelectric origin (electromagnons) exist.[14] As shown previously, the electromagnons are magnons that can be excited by the electric component of the electromagnetic wave. These excitations are suppressed in the CA-AFM state, e.g., in external magnetic fields along the *c* axis. It is the aim of this work to study the magnetic-field and temperature dependence of electromagnons in a broad frequency range and to investigate their coupling to phonon modes.

The lower panel of Fig. 1 shows the reflectance spectrum of GdMnO$_3$ at phonon frequencies and for the ac electric field component $\tilde{e}$ parallel to the crystallographic *a* axis. We note that this direction of the electric field reveals large effects in the temperature and field dependence of the dielectric constant[6] and is especially important for the magnetodielectric effects in this compound. The solid line in the lower panel of Fig. 1 has been calculated using a sum of 15 Lorentzians. Here the ten strongest excitations correspond to phonons polarized along the *a* axis at frequencies 119, 188, 231, 308, 325, 400, 460, 475, 509, and 568 cm^{-1}. Weaker features at 296, 441, 539, and 641 cm^{-1} are due to leakage of the *b* axis component, most probably because of a small
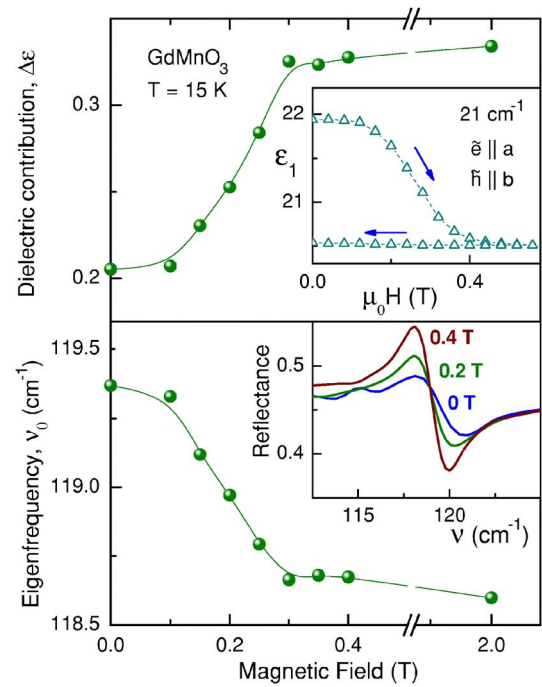

FIG. 2. (Color online) Magnetic-field dependence of the parameters of the phonon at 119 cm^{-1} crossing the boundary between IC-AFM and CA-AFM phases. Upper panel: dielectric contribution ($\Delta\varepsilon$). Lower panel: eigenfrequency (ν_0). The lower inset shows the reflectance spectra at typical magnetic fields. The upper inset shows the changes in dielectric permittivity at a frequency close to the electromagnon, which demonstrates a direct connection of the two effects.

misorientation of the crystal. The origin of the weak excitation at 76 cm^{-1} is presently unknown.

Except for the lowest-frequency phonon at 119 cm^{-1}, no measurable changes in the phonon parameters have been detected between different magnetic phases. On the contrary, the 119 cm^{-1} phonon, which is observed for *a*-axis polarization only, reveals substantial changes between the IC-AFM and CA-AFM phases. We recall that the peculiarity of this transition into the CA-AFM phase is the occurrence of strong magnetodielectric effects, e.g., the magnetic-field dependence of the *a*-axis dielectric constant in the frequency range from zero to about 1 THz ($\sim$40 cm^{-1}).[14] Similar to other perovskite manganites, the lowest phonon mode at 119 cm^{-1} is probably of external character. The similarity of excitation conditions ($\tilde{e}\|a$) and the closeness of frequency positions seem to be the main reasons for the coupling of electromagnons with this phonon.

The magnetic-field dependence of the 119 cm^{-1} phonon excitation on crossing the IC-CA magnetic phase boundary is shown in the lower inset of Fig. 2, which represents the reflectance spectra at three typical fields. The dielectric contribution ($\Delta\varepsilon$, strength of the mode) and the eigenfrequency (ν_0) of the phonon are shown in the main panels. The transition is manifested by a softening of the phonon frequency and by a 60% increase of the mode strength on increasing the magnetic field. The characteristic fields and the width of the transition closely coincide with the corresponding changes of the dielectric constant at lower frequency, which are demon-
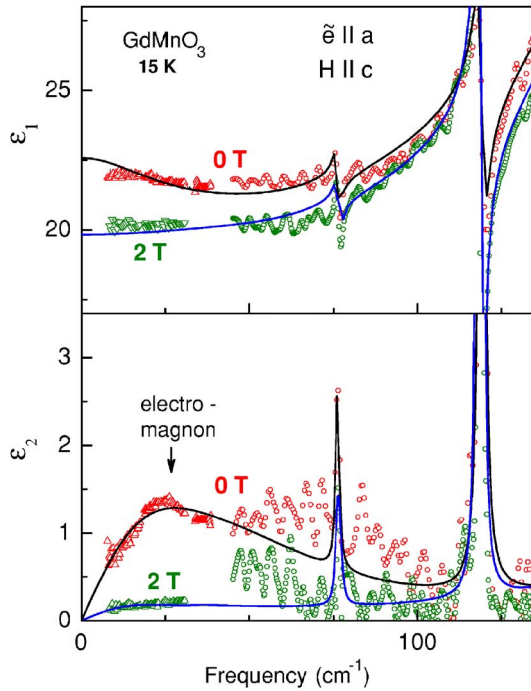
FIG. 3. (Color online) Spectra of the *a*-axis dielectric permittivity of GdMnO$_3$ in the frequency range between the electromagnon at 25 cm^{-1} and the phonon at 119 cm^{-1} at 0 T (incommensurate state) and 2 T (canted state). Upper panel: real part of the dielectric permittivity. Lower panel: imaginary part. Triangles represent the results from the terahertz transmittance. Circles are spectra obtained via Kramers-Kronig analysis of the reflectance. Solid line corresponds to a sum of Lorentzians as described in the text.

strated in the upper inset of Fig. 2. The difference in ε_1 on increasing and decreasing fields documents the metastable character of the IC-CA phase boundary. Similar behavior of the high- and low-frequency dielectric constant indicates that the same mechanism is operative for both effects, namely, that at the IC-CA transition electromagnons are suppressed by the external magnetic field.[14]

In order to analyze the interplay between electromagnons and phonons the complex dielectric permittivity has been calculated from the reflectance spectra via the Kramers-Kronig transformation by adding the terahertz spectra at low frequencies. The results both in the IC-AFM (15 K, 0 T) and in the CA-AFM (15 K, 2 T) state are shown in Fig. 3. Here the data above 40 cm^{-1} represent the results of the Kramers-Kronig analysis and the data below this frequency have been taken directly from the terahertz transmittance experiments. The lower panel of Fig. 3 clearly demonstrates the overdamped, almost relaxational, nature of the electromagnon and its suppression by the external magnetic field. On the other hand, we know from Fig. 2 that the phonon mode at 119 cm^{-1} gains considerable spectral weight (SW) on increasing the magnetic field. The substantial SW that is removed from the low-frequency range is transformed into phonon intensity at 119 cm^{-1}. In order to obtain an estimate of the SW transfer, the complex dielectric permittivity has been fitted assuming the phonon parameters as obtained from the fits of the reflectance and a single overdamped Lorentz-
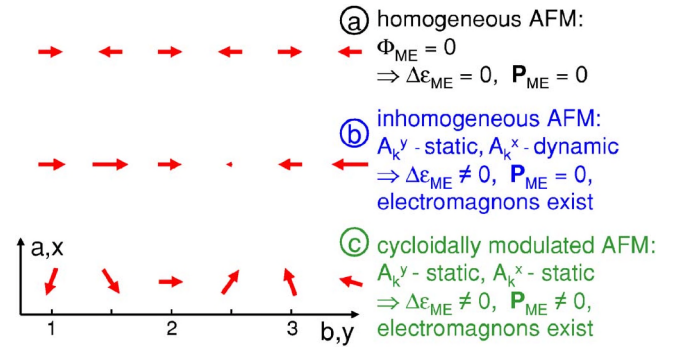

FIG. 4. (Color online) Schematic presentation of magnetic structures, showing different magneto-electric behavior. (a) Homogeneously modulated structure: no static electric polarization (ΔP_{ME} =0), no ME contribution to the dielectric permittivity ($\Delta\varepsilon$=0). (b) Inhomogeneously modulated collinear structure: no electric polarization, but nonzero contribution to the dielectric permittivity. (c) Cycloidally modulated structure: finite electric polarization and ME contribution to the dielectric permittivity.

ian representing the electromagnon with $\Delta\varepsilon$=1.6 and the maximum in ε_2 at $\nu_{max} \simeq 27$ cm^{-1}. From these data the SW of the electromagnon $S = \Delta\varepsilon\,\nu_{max}^2 \simeq 1.2 \times 10^3$ cm^{-2}. From the parameters in Fig. 2 the SW increase of the phonon is obtained as $S_{CA} - S_{IC}$. Taking into account strong scattering of the data between 40 and 100 cm^{-1}, which does not allow direct integration of the SW, we conclude a rough coincidence of these values and the transformation of the spectral weight of the electromagnon into the phonon mode at 119 cm^{-1}.

A remaining question is why electromagnons are observed both in GdMnO$_3$, in a nonferroelectric collinear magnetic structure, as well as in TbMnO$_3$, in a ferroelectric with helical spin structure.[14] In order to understand this point, Fig. 4 provides a closer inspection of the free ME energy in terms of the Fourier components of the dynamic variables $\mathbf{A}_k$ related to the base AFM vector $\mathbf{A}$ of the modulated spin structure[18] (see also Refs. 7 and 12):

$$\Phi_{ME} = -iP_x\sum_k a_k^{xz}(\mathbf{A}_k \times \mathbf{A}_k^*)_z - iP_z\sum_k a_k^{zx}(\mathbf{A}_k \times \mathbf{A}_k^*)_x$$

$$\equiv -\sum_k \mathbf{P}\mathbf{E}_{int}(\mathbf{A}_k), \tag{1}$$

where $\mathbf{P}$ is the electric polarization. The ME coefficients $a_k^{xz,zx}$ for the nearest neighbors within the *ab* plane are determined by $a_k^{xz,zx} = 2Na^{xz,zx}\cos(2\pi kb)\sin(\pi kb)$, where $a^{xz,zx}$ are constants, N the number of Mn ions, and b the lattice constant. This expression was derived using the crystallographic symmetry D_{2h}^{16} (*Pbnm* space group) and a modulated spin structure with $\mathbf{k} = (0, k, 0)$. We omitted weak contributions from other AFM vectors $\mathbf{F}$, $\mathbf{C}$, $\mathbf{G}$,[18] which exist in this structure. In space representation and the continuum limit Eq. (1) corresponds to $\Phi_{ME} = -a_x P_x(A_x \partial A_y/\partial y - A_y \partial A_x/\partial y) - a_z P_z(A_z \partial A_y/\partial y - A_y \partial A_z/\partial y)$,[14] and for $a_k^{xz} = a_k^{zx}$ is reduced to Dzyaloshinski-Moriya-type interactions.[9–11]

It is clear that in a homogeneous magnetic state, as in the CA-AFM phase [Fig. 4(a)], the ME free energy is zero and

no contribution to the dielectric constant, no electromagnons, and no spontaneous polarization can exist. To obtain the ME contribution to the electric susceptibility in sinusoidal and spiral states we consider the total free energy of the system:

$$\Phi(\mathbf{A}_k, \mathbf{P}) = \frac{1}{2} N \sum_k \left[-J_A(k) \mathbf{A}_k \mathbf{A}_k^* + K_{bc} \mathbf{A}_k^z \mathbf{A}_k^{z*} + K_{ba} \mathbf{A}_k^x \mathbf{A}_k^{x*} \right]$$
$$- \mathbf{E} \cdot \mathbf{P} + \mathbf{P}^2/2\chi_E + \Phi_{ME} - TS(\mathbf{A}_k), \qquad (2)$$

where the first three terms correspond to exchange and anisotropy energies, the fourth and fifth terms represent dielectric contributions from external electric fields $\mathbf{E}$, and the last term is the spin entropy. By minimizing Eq. (2) with respect to $\mathbf{P}$ the free energy can be represented as a function of the nonequilibrium values of $\mathbf{A}_k$. In a sinusoidal spin structure with $\mathbf{A}_k = (0, \mathbf{A}_k^y, 0)$ and keeping only the main harmonic k_0 of the modulated structure, the electric susceptibility, e.g., along the a axis, can be expressed as

$$\chi_E^x \approx -\partial^2\Phi/\partial E_x^2 + (\partial^2\Phi/\partial E_x \partial A_k^x)$$
$$\times (\partial^2\Phi/\partial E_x \partial A_k^{x*})/(\partial^2\Phi/\partial A_k^x \partial A_k^{x*})$$
$$\approx \chi_E + (\chi_E a_{k0}^{xz})^2 A_{k0}^y A_{k0}^{y*}/K_{ba}. \qquad (3)$$

In the sinusoidal phase no spontaneous polarization can exist since only one $\mathbf{A}_k$ component is nonzero, but the ME contribution to the electric susceptibility arises according to Eq. (3). It originates from an electric-field-induced rotation of the spins in the ab plane, i.e., from the $\mathbf{A}_k^x$ spin components. Similar contribution can also exist along the c axis. Finally, in Fig. 4(c) with helical or cycloidally modulated spins, e.g., $\mathbf{A}_k = (0, \mathbf{A}_k^y, \mathbf{A}_k^z)$, a spontaneous ferroelectric polarization

along the c axis P_z, a finite contribution to the dielectric constant along the a axis $\chi_E^x \approx \chi_E + (\chi_E a_{k0}^{xz})^2 S^2/K_{ba}$, and electromagnons exist.

Very recently Katsura *et al.*[13] calculated the collective mode dynamics of helical magnets coupled to the electric polarization. For the ac dielectric properties their main findings are the occurrence of two modes, one of which is derived from the phonon mode with a frequency close to the eigenfrequency of the uncoupled phonon, and one originating from the spin wave with a frequency proportional to $\sqrt{SJD}$, where S is the spin value, J the exchange coupling, and D the anisotropy. Using realistic parameters they calculate an electromagnon frequency of $\nu_p \sim 10$ cm^{-1}, close to the experimental observation. It also follows from their calculation that in the electromagnetic phase the phonon eigenfrequency (ν_0) is enhanced by $\nu_p^2/2\nu_0$, which from the lower panel of Fig. 2 gives a similar estimate $\nu_p \simeq 13$ cm^{-1}. Finally, we note that the calculations of Ref. 13 were done for a spiral magnetic ground state and therefore cannot be applied to GdMnO$_3$ straightforwardly.

In conclusion, by studying the low-frequency electrodynamics of GdMnO$_3$ with a finite magnetoelectric coupling, we were able to demonstrate (i) the existence of electromagnons, (ii) that these collective modes of ME magnets contribute to the static dielectric constant, and (iii) that at the transition to a homogeneous magnetic phase the spectral weight of electromagnons is transferred to an optical phonon, which in addition reveals a slight softening of the eigenfrequency.

[1] N. A. Hill, J. Phys. Chem. B **104**, 6694 (2000).

[2] M. Fiebig, J. Phys. D **38**, R123 (2005).

[3] D. Khomskii, J. Magn. Magn. Mater. **306**, 1 (2006).

[4] J. Hemberger, P. Lunkenheimer, R. Fichtl, H.-A. Krug von Nidda, V. Tsurkan, and A. Loidl, Nature (London) **434**, 364 (2005).

[5] T. Kimura, T. Goto, H. Shintani, K. Ishizaka, T. Arima, and Y. Tokura, Nature (London) **426**, 55 (2003).

[6] T. Kimura, G. Lawes, T. Goto, Y. Tokura, and A. P. Ramirez, Phys. Rev. B **71**, 224425 (2005).

[7] M. Kenzelmann, A. B. Harris, S. Jonas, C. Broholm, J. Schefer, S. B. Kim, C. L. Zhang, S.-W. Cheong, O. P. Vajk, and J. W. Lynn, Phys. Rev. Lett. **95**, 087206 (2005).

[8] T. Arima, A. Tokunaga, T. Goto, H. Kimura, Y. Noda, and Y. Tokura, Phys. Rev. Lett. **96**, 097202 (2006).

[9] H. Katsura, N. Nagaosa, and A. V. Balatsky, Phys. Rev. Lett. **95**, 057205 (2005).

[10] M. Mostovoy, Phys. Rev. Lett. **96**, 067601 (2006).

[11] I. A. Sergienko and E. Dagotto, Phys. Rev. B **73**, 094434 (2006).

[12] G. Lawes, A. B. Harris, T. Kimura, N. Rogado, R. J. Cava, A. Aharony, O. Entin-Wohlman, T. Yildirim, M. Kenzelmann, C. Broholm, and A. P. Ramirez, Phys. Rev. Lett. **95**, 087205 (2005).

[13] H. Katsura, A. V. Balatsky, and N. Nagaosa, cond-mat/0602547 (unpublished).

[14] A. Pimenov, A. A. Mukhin, V. Yu. Ivanov, V. D. Travkin, A. M. Balbashov, and A. Loidl, Nat. Phys. **2**, 97 (2006).

[15] J. Hemberger, S. Lobina, H.-A. Krug von Nidda, N. Tristan, V. Yu. Ivanov, A. A. Mukhin, A. M. Balbashov, and A. Loidl, Phys. Rev. B **70**, 024414 (2004).

[16] T. Goto, T. Kimura, G. Lawes, A. P. Ramirez, and Y. Tokura, Phys. Rev. Lett. **92**, 257201 (2004).

[17] A. A. Volkov, Yu. G. Goncharov, G. V. Kozlov, S. P. Lebedev, and A. M. Prochorov, Infrared Phys. **25**, 369 (1985); A. Pimenov, S. Tachos, T. Rudolf, A. Loidl, D. Schrupp, M. Sing, R. Claessen, and V. A. M. Brabers, Phys. Rev. B **72**, 035131 (2005).

[18] E. F. Bertaut, in *Magnetism*, edited by T. Rado and H. Suhl (Academic, New York, 1963), Vol. III, p. 149.